We are IntechOpen, the world's leading publisher of Open Access books Built by scientists, for scientists

6,900
Open access books available

186,000
International authors and editors

200M
Downloads

Our authors are among the

154
Countries delivered to

TOP 1%
most cited scientists

12.2%
Contributors from top 500 universities

WEB OF SCIENCE™

Selection of our books indexed in the Book Citation Index in Web of Science™ Core Collection (BKCI)

Interested in publishing with us?
Contact book.department@intechopen.com

Numbers displayed above are based on latest data collected.
For more information visit www.intechopen.com

5

Real-Time Analysis of Intracranial Pressure Waveform Morphology

Fabien Scalzo, Robert Hamilton and Xiao Hu
Neural Systems and Dynamics Laboratory (NSDL), UCLA
USA

1. Introduction

The cranial vault is composed of four fundamental components: arterial blood, venous blood, cerebrospinal fluid (CSF), and brain parenchyma. Intracranial pressure (ICP) represents the pressure within the brain parenchyma and cerebrospinal fluid (CSF). The environment within the cranial vault is unique compared to other organ systems; it is enclosed within a rigid skull and thus small volumetric changes in any of the four elements lead to significant changes in ICP. One example of this, is the periodic influx of arterial blood over the cardiac cycle; this change causes the ICP pulse pressure waveform. The pulse pressure waveform has three characteristic peaks hypothesized to correspond to different physiologic components. Early work [1] demonstrated the relationship between pulsations in the choroid plexus and the pulse pressure waveform. Moreover, other studies [2] compared the right atrium (venous) and the aortic (arterial) pressures to the intracranial waveform in the cistern magna and showed that although the cranial pulse pressure is related to arterial pulsations, there is also a venous component. The results of these studies support the current theories for the etiology of the characteristic peaks in the ICP pulse pressure waveform. The majority of the literature indicates that P1, the percussion wave, corresponds with the pulsation of the choroid plexus and/or large intracranial conductive vessels [3-5]. The rebound of the percussion wave is thought to contribute to P2, which has also been related to cerebral compliance [5]. Finally, the dicrotic wave, or P3, is thought to be venous in origin [2, 4, 6].

ICP monitoring is fundamental to the management of numerous intracranial pathologies, including the management of traumatic brain injury (TBI), subarachnoid hemorrhage (SAH), hydrocephalous, and any other conditions where pathological changes in intracranial volume (ICV) may occur. Maintaining an ICP within normal limits is vital for adequate perfusion of the brain. An increase in ICP (intracranial hypertension) reduces arterial blood flow into the cranial vault, while decreased ICP (intracranial hypotension) results in severe headaches. Although the importance of monitoring ICP is well established, only recently has ICP pulse pressure waveform morphology yielded promising results due to advancing technology. However, the importance of ICP pulse pressure waveform morphology has been known for years; special interest should be focused not only on the height of mean ICP, but also on the pressure pulse curve, because the configuration and pulse amplitude of the CSF pulsations can be regarded to a certain extent as an index of the state of intracranial elastance or cerebral bulk compliance [6].

Methods for monitoring ICP include: epidural, subarachnoid, intraventricular, and intraparenchymal pressure probes. For the investigation of ICP morphology, a continuous measurement of ICP must be achieved. There have been several recent advances by various groups to analyze continuous ICP waveform morphology. An analysis method [7] that utilizes 6-sec time windows to extract average amplitude and latency information for the given window was developed. Our group has recently developed a time-domain analysis toolbox for intracranial waveform morphology known as Morphological Clustering and Analysis of Continuous Intracranial Pulse (MOCAIP)[8]. The details of this algorithm will be presented in the subsequent chapter. Several groups have successfully utilized pulse pressure waveform morphology analysis in the diagnosis and management of various conditions. For example, pulse pressure amplitude has been linked to several conditions with promising results in normal pressure hydrocephalus (NPH) for predicting shunt responsiveness [9, 10]. Work has also been done in chronic headaches; again, showing the usefulness of pulse pressure amplitude. Furthermore, our group has investigated several conditions using ICP morphological metrics including: detection of cerebral hyoperfusion [11], prediction of ICP hypertension [12], segmentation of ICP slow waves [13], changes in vasoreactivity (vasodilatation) [14]. ICP monitoring has been fundamental for the diagnosis and management of several conditions for decades. In this chapter, we present a few of the recent advances in the analysis of ICP pulse pressure waveforms and its applications as described above.

2. Automatic analysis of ICP morphology

As previously described, the ICP pulse pressure signal contains three characteristic peaks [5]. From those peaks, it is possible to describe in a parametric way the amplitude and timing information of the pulse for further examination. While several studies have focused on the offline analysis of the ICP waveform [15-17] and the extraction of its morphological features, processing ICP signals to extract the three peaks in a continuous way is challenging because the signal is commonly affected by various types of noise and artifacts. MOCAIP algorithm [18, 19] was developed by our group to address these issues. MOCAIP is capable of extracting morphological features of ICP pulses in real-time by recognizing legitimate ICP pulses, and by detecting the three peaks from average waveforms computed from segments of ICP.

Recently, two main extensions have been developed from the original framework. MOCAIP++ (Section 2.1) is a generalization of MOCAIP that allows different peak recognition techniques to be used and uses intermediate features to make the peak detection more robust to the variations observed in the clinical conditions. The latest extension of MOCAIP is presented in Section 2.2 and poses the peak detection problem in terms of Bayesian inference.

2.1 MOCAIP++

MOCAIP++ [20] generalizes MOCAIP in two ways. First, it proposes a unifying framework where different peak recognition techniques can be integrated. Second, it allows the algorithm to take advantage of additional ICP features to improve the peak recognition. A summary of the algorithm is described in the following subsections.

ICP Segmentation: The continuous raw ICP signal is segmented into a series of individual ICP pulses using a pulse extraction technique [21] combined with the ECG QRS detection [17, 22] that locates each ECG beat. Because ICP recordings are subject to various noise and artifacts during the acquisition process, an average pulse is extracted from a series of consecutive ICP pulses using hierarchical clustering [23].

Peak Candidates: Peak candidates, each being a potential match to one of the three peaks, are detected at curve inflections of the average ICP pulse using the second derivative of the signal.

Second-order ICP Features: We have shown in a recent study [20] that the first derivative of the ICP signal is very useful to discriminate between ICP peaks and therefore preoviding improve recognition. In our previous work, the first L_x demonstrated the best improvements in comparison with the second derivative and the curvature within MOCAIP++ framework. The derivative L_x is computed according to the smoothed version L of the ICP,

$$L_x = L(x,\sigma) - L(x+1,\sigma). \tag{1}$$

where the ICP signal $I(x)$ is first convolved with a Gaussian smoothing filter $G(x;\sigma)$ with the standard deviation σ to generate $L(x,\sigma)$,

$$L(x,\sigma) = G(x;\sigma) * I(x). \tag{2}$$

Peak Recognition: The peak recognition tasks consists in recognizing the three peaks (p_1, p_2, p_3) among the set of candidate peaks detected within the pulse. Several techniques have been developed and can be used such as independent Gaussian models [18], Gaussian Mixture Models (GMM), and spectral regression (SR) analysis [19]. Depending on the technique, it can exploit the latency of the peak candidates, the raw ICP pulse, or different features extracted from the pulse.

Morphological metrics: Once the peaks have been detected in an ICP pulse, a set of metrics (Fig. 1) is used to describe the shape morphology in a parametric way. This allows to obtain a better understanding about the type of variations that take place.

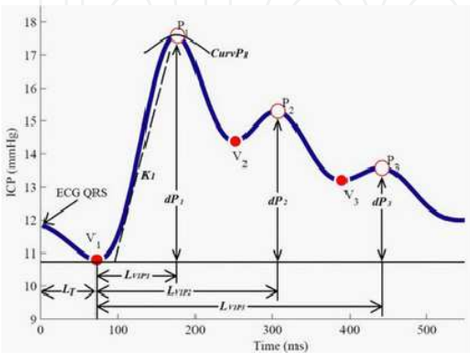

28 Basic metrics extracted from individual landmarks or over all characteristics	
dV1, dV2, dV3, dP1, dP2, dP3	Amplitude of landmark relative to the minimum point prior to initial rise
L_{V1P1}, L_{V1P2}, L_{V1P3}, L_{V2P2}, L_{V3P3}	Time delay among landmarks
$Curv_{v1}$, $Curv_{v2}$, $Curv_{v3}$, $Curv_{p1}$, $Curv_{p2}$, $Curv_{p3}$	Absolute curvature of each landmark
K1, K2, K3, RC1, RC2, RC3	K1, K2, K3 are slope of each rising edge and RC1, RC2, RC3 are time-constants of each descending edge
mICP, diasICP	Mean ICP and diastolic ICP
L_T	Time delay of V_1 to ECG QRS peak
mCurv	Mean absolute curvature of the pulse
WaveAmp	Maximum among dP1–dP3
100 extended metrics calculated as ratios among metrics within each group	
$dP_{p1p2,...}$	Ratio among landmark amplitudes
$L_{V1P1}/L_{T,...}$	Ratio among time delays
$Curv_{v1}/Curv_{v2,...}$	Ratio among curvatures
$K_1/RC_{1,...}$	Ratio among slopes/RCs

Fig. 1. Illustration of morphological metrics extracted From ICP peaks (reproduced with permission from [14] and [66]).

2.2 Bayesian tracking of ICP morphology

In this section, we present a probabilistic framework [24] to track ICP peaks in real time. The tracking is posed as inference in a graphical model that associates a continuous random variable to the position of each of the three peaks, in terms of their latency within the pulse and pressure level. The model (Section 2.3) represents the dependencies between the peaks using a Kernel Density Estimation (KDE) from evidence collected from manually annotated pulses, while Nonparametric Belief Propagation (NBP) [25] is used during the detection process (Section 2.4).

We assume that the tracking framework is presented with a series of raw pulses extracted from the ICP signal. The model consists of three distinct states $[x_{t,1}, x_{t,2}, x_{t,3}]$ at time t, one for the position of each peak. A state $x_{t,i} = \{\mu_{t,i}, v_{t,i}\}$ is two-dimensional that defines the latency $\mu_{t,i} \in R$, and the ICP elevation $v_{t,i} \in R$ of the peak. To each state $x_{t,i}$ is associated an observation $y_{t,i}$ directly extracted from the position of the peak within the current pulse.

2.3 Probabilistic tracking framework

The graphical model used in our tracking framework defines relations between pairs of nodes. States $x_{t,i} \in x$ and observations $y_{t,i} \in y$ are represented in the graphical model and illustrated in Fig. 2 by white, and shaded nodes, respectively. Edges represent dependencies between states, and possibly observations, by two types of functions: observation potentials $\phi(x_{t,i}, y_{t,i})$ that are the equivalent of the likelihood part $p(y_{t,i} \mid x_{t,i})$, and compatibility potentials $\psi_{ij}(x_{t,i}, x_{t,j})$ that embed the conditional parts $p(x_{t,i} \mid x_{t,j})$, $p(x_{t,j} \mid x_{t,i})$ of the Bayesian formulation and can be used by conditioning them in either directions during inference. By introducing compatibility potentials between states of the same peak at successive times $\psi(x_{t,i}, x_{t-1,i})$, that we name temporal potentials, the model becomes a dynamic Markov model.

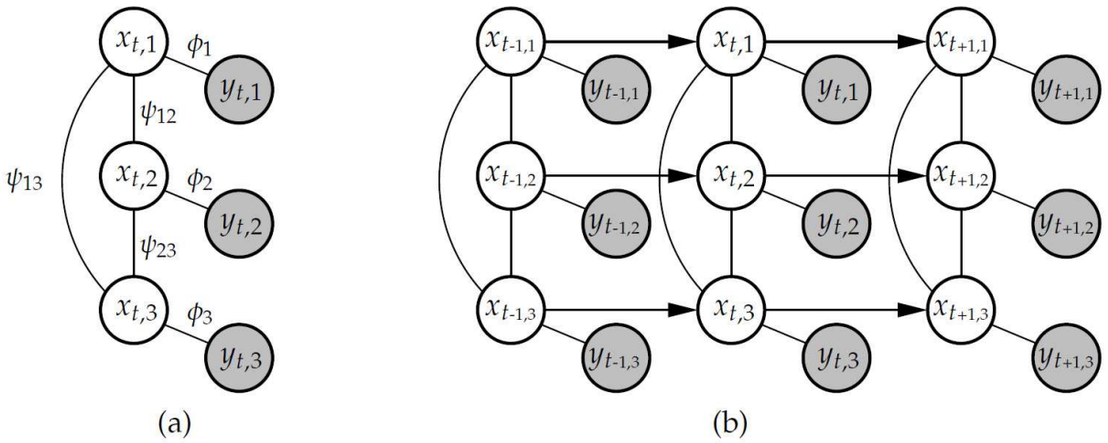

Fig. 2. The graphical model represents the dependence through pairwise potentials $(\psi_{12}, \psi_{13}, \psi_{23})$ between hidden nodes (x_1, x_2, x_3), and likelihood functions (ϕ_1, ϕ_2, ϕ_3) between hidden and observable nodes (y_1, y_2, y_3) (a). By introducing temporal potentials between successive nodes (b), the graphical model becomes dynamic and allows for tracking ICP peaks in real time (reproduced from permission from [24]).

2.3.1 Observation model

An observation $y_{t,i} \in \{R^2 \cup \varnothing\}$ corresponds to the position of the i^{th} peak, in terms of latency and ICP elevation, that was produced by a peak detector at time t. Our framework uses MOCAIP as peak detector but any other peak detection technique can be used within our model. Observations $y_{t,i}$ are linked to their state $x_{t,i}$ through an observation potential $\phi(x_{t,i}, y_{t,i})$. Equation (3) formalizes the integration of the observation using a Gaussian model,

$$\phi(x_{t,i}, y_{t,i}) = \begin{cases} exp(-\alpha^{-1} \mid y_{t,i} - x_{t,i} \mid^2), if(y_{t,i} \neq \varnothing) \\ \lambda_i, if(y_{t,i} = \varnothing) \end{cases} \tag{3}$$

where α is a smoothing parameter, and λ_i is a constant factor that accounts for missing peaks by the detector.

2.3.2 Compatibility and Temporal potentials

Temporal potentials $\psi(x_{t-1,i}, x_{t,i})$ define the relationship between two successive states of a peak. They are defined as a Gaussian difference between their arguments,

$$\psi(x_{t-1,i}, x_{t,i}) = exp(-\mid x_{t-1,i} - x_{t,i} \mid^2 / \sigma_t^2) \tag{4}$$

where the standard deviation σ_t of the model was previously estimated using maximum likelihood (ML) on training data. Compatibility potentials $\psi_{i,j}(x_{t,i}, x_{t,j})$, however, are not expected to follow a Gaussian distribution. Each potential is represented by a KDE [26] $\psi_{i,j}(x_{t,i}, x_{t,j}) = \hat{f}(x_{ij}; \Theta)$ that is constructed by collecting co-occurring ICP peak positions across the training set.

2.4 Tracking ICP peaks using nonparametric bayesian inference

Detecting peaks in an ICP pulse at time t amounts to estimating $p(x_t \mid y_{\{1...t\}})$, the posterior belief associated with the states $x_t = \{x_{t,1}, x_{t,2}, x_{t,3}\}$ given all observations $y_{\{1...t\}} = \{y_{\{1...t\},1}, y_{\{1...t\},2}, y_{\{1...t\},3}\}$ accumulated so far. Thus, peak detection is achieved through inference in our graphical model. One way to do this efficiently is to use Nonparametric Belief Propagation [25]. It is a message passing algorithm for graphical models that generalizes particle filtering and Belief Propagation (BP). Messages are repeatedly exchanged between nodes to perform inference. Following the notation of BP, a message m_{ij} sent from node i to j is written [1],

$$m_{i,j}(x_j) \leftarrow \int \psi_{i,j}(x_i, x_j)\, \phi_i(x_i, y_i) \prod_{k \in N_i \setminus j} m_{k,i}(x_i) dx_i \tag{5}$$

[1]To simplify the notation, we discard the temporal subscript t of each node which is not necessary to explain the inference.

where $N_{i\setminus j}$ is the set of neighbors of state i where j is excluded, $\psi_{i,j}(x_i, x_j)$ is the pairwise potential between nodes i, j, and $\phi_i(x_i, y_i)$ is the observation potential. Each message $m_{i,j}(x_j)$ as well as each node $x_i \in x$ distribution is represented through a multivariate KDE.

To compute an outgoing message $m_{i,j}(x_j)$, NBP requires the pairwise potential $\psi_{i,j}(x_i, x_j)$, which represents the joint distribution between the nodes, to be conditioned on the source state x_i. This task is achieved by sampling N_a particles $s_j^k \leftarrow \psi_{i,j}(x_i = s_i^k, x_j)$ from the potential.

After any iteration of message exchanges, each state can compute an approximation $\hat{p}(x_i \mid y_{\{1\ldots t\}})$, called belief, to the marginal distribution $p(x_i \mid y_{\{1\ldots t\}})$ by combining the incoming messages with the local observation:

$$\hat{p}(x_i \mid y_{\{1\ldots t\}}) \leftarrow \phi_i(x_i, y_i) \prod_{k \in R_i} m_{k,i}(x_i) \tag{6}$$

An example of inference is provided in Fig. 3 where the latency and the elevation of the three peaks is tracked simultaneously and in real-time on a pulse-by-pusle fashion.

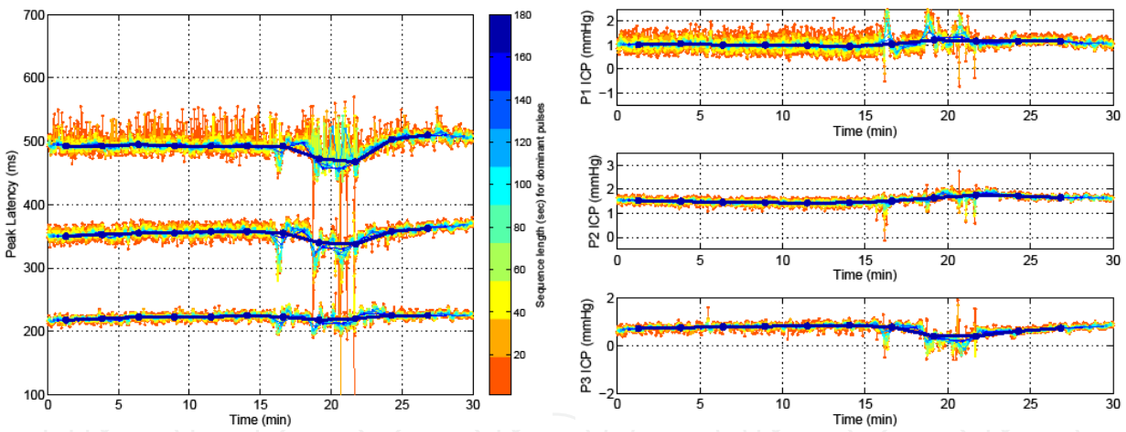

Fig. 3. Peak latency (left) and ICP elevation (right) estimated on ICP sequences by NBP tracking algorithm. The predictions of the tracking are obtained in real-time and are robust to transient perturbations that frequently occur during the ICP signal recording.

3. Detection of decreased cerebral blood flow (CBF)

The measure of cerebral blood flow (CBF) is an indicator of perfusion and is therefore very useful in neurocritical care. While imaging techniques provide a snapshot in time and invasive monitors offer continuous readings of the CBF, they usually carry additional risks and require additional equipments and increased cost. Furthermore, non-invasive techniques for CBF monitoring only provide intermittent measures of CBF. There is therefore a need to create a continuous, low cost technique that would not increase risk and could be easily integrated to bedside monitors.

Drawing from the fact that a physiological relation exists between ICP and CBF, we recently investigated if the ICP signal holds predictive information about CBF. Such a complex relationship has only been partially explored such that mean ICP (mICP) is used in the following equation to derive the driving pressure of blood flow through the cerebral vasculature:

$$CPP = ABP - mICP \tag{7}$$

where CPP stands for cerebral perfusion pressure, and ABP for systemic arterial blood pressure (ABP). To date, the influence of cerebral vascular changes on both ICP and CBF remain poorly understood. Subtle changes in the morphology of ICP pulses may reflect cerebral vascular changes. Because an ICP waveform can be thought as arising from an incidental arterial pressure pulse influenced by different intracranial compartments, we hypothesize that the ICP waveform carries information composed of changes in cerebral vasculature and hence CBF. In this section, we report our study [11] investigating the ability of ICP morphoology metrics to detect low CBF. A multi-modal dataset originating from brain injured patients with ICP monitoring, global average CBF, and Transcranial Doppler (TCD) assessment was analyzed. Detection of low CBF was posed as a classification problem and implemented using a regularized linear discriminant analysis (LDA). To further improve the performance of the framework, an optimization algorithm was used to find the subset of morphological metrics that maximizes a measure based on the combination of positive predictivity and sensitivity.

3.1 Data

The dataset used in our study originates from 63 patients among which 31 were admitted for SAH from aneurysm rupture and 26 had a TBI. The remaining patients were admitted either with arteriovenous malformation, brain tumor, and Intraparenchyma hemorrhage.

The mean global CBF was measured using the intravenous ^{133}Xenon clearance technique [27] for 11 minutes. TCD [28] was used to insonate the extracranial internal carotid artery (ICA) and the basilar artery (BA). Blood samples were taken immediately before or after CBF measurement. In addition to ECG, ICP was monitored using ventriculostomy and waveforms were recorded from bedside monitors at a sampling rate of 240 Hz. The ICP signal (selected as a one hour segment closest to the CBF measurement) was processed by MOCAIP to extract 24 morphological metrics for each three minute segment of data. A total number of 199 CBF-TCD-ICP segments were extracted from the 63 patients. In addition to the 24 morphological metrics extracted from ICP, the eight following variables weren also extracted: 1) average flow velocities of the right and the left internal carotid artery (ICA); 2) average diastolic flow velocities of the right and the left ICA; 3) average pulsatility indices (PI) of the right and the left ICA; 4) partial carbon dioxide pressure (CO_2); 5) total amount of hemoglobin (Hgb); 6) fraction of the blood composed of red blood cells (Hct); 7) mean arterial blood pressure (MAP); 8) amount of CSF drainage in the hour of CBF measurement.

3.2 Experiments

A classification experiment was designed to evaluate the power of ICP morphology to discriminate between low and normal CBF value (averaged globally, threshold of 20 ml/min/100g). Four combinations of all 32 available metrics were considered, within which an optimal subset was obtained using the classifier training algorithm described below; with (a) all 32 metrics, (b) only includes MOCAIP, CSF drainage and TCD metrics, (c) only morphological ICP and CSF drainage metrics, and (d) only seven TCD and blood analysis metrics. Using those features, a regularized version [29] of the Gaussian quadratic classifier (QDC) was chosen, and differential evolution (DE) [30] used to optimize the model using feature selection. The objective function for the optimization algorithm is the average of the sensitivity and the positive predictivity (PPV). Each evaluation of the objective function involves a leave-one-patient-out cross-validation.

3.3 Results

A sensitivity of $81.8 \pm 0.9\%$ and specificity of $50.1 \pm 0.2\%$ were obtained using the optimal combination (d) of conventional TCD and blood analysis metrics as input. Using the optimal combination of the morphological metrics alone (c) was able to achieve a sensitivity of $92.5 \pm 0.7\%$ and specificity of $84.8 \pm 0.8\%$. Searching for the optimal combination of all available metrics (a) achieved the best result that was marginally better than those from using morphological metrics alone (c). To visually assess how ICP pulse morphology is associated with different perfusion states, we present one typical case in Fig. 4 from a traumatic brain injury patient who had ICP recordings both in the normal and in the low CBF states. In each plot, we overlap the average ICP pulses extracted from every three minutes of data. In addition, we display the CBF value associated with the ICP recording. We observe that the elevation of the third peak within the pulse is associated with low CBF value. This pattern of elevated third peak was observed in six out of the eight patients with positive cases.

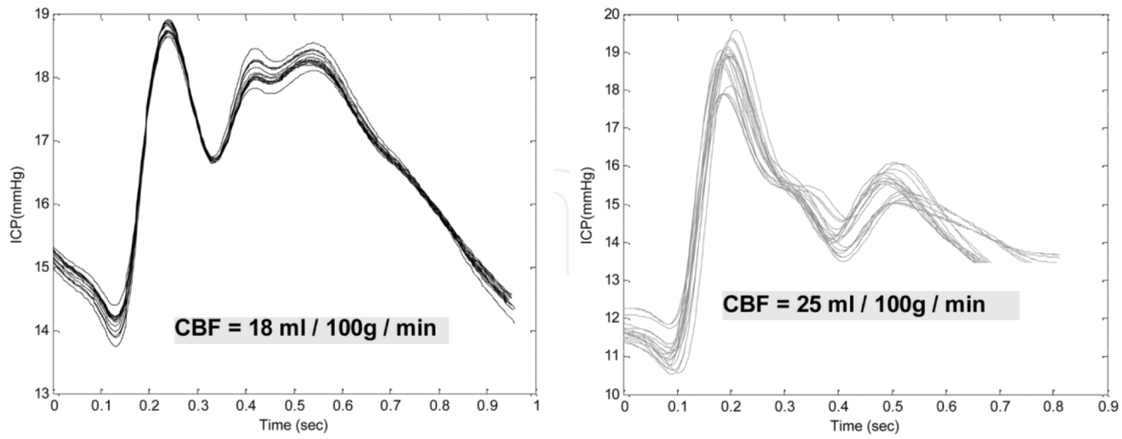

Fig. 4. Illustration of average ICP pulse with low (left) and normal (right) CBF (reproduced with permission from [11]).

Table 1 lists the mean and standard deviation of sensitivity, specificity, and positive predictivity value of the three after the leave-one-out (LOO) cross-validation and the bootstrapping (BS) cross-validation. Based on the bootstrapping results, it is observed that

combining morphological ICP metrics, TCD, and blood analysis achieves the best performance. The biggest gain of the performance is caused by the incorporation of the morphological ICP metrics. The number of times each metrics was selected over the experiment was accumulated and analyzed. The following metrics were always selected; dP_{13}, dP_3, diasP, mICP, L_t, L_3, and ICAEd. There are 10 more metrics, including ICAPI and Hct, were selected for majority of the runs. Also, there are 10 metrics that were never selected as part of classifier features including PCO_2, Hgb, and ICAMean. The complete list of the metrics can be found in the original paper.

Exp.	Val.	SE	SPE	PPV
MOCAIP+TCD+BA	LOO	0.933 ± 0.000	0.862 ± 0.003	0.356 ± 0.005
	BS	0.941 ± 0.014	0.852 ± 0.013	0.341 ± 0.024
MOCAIP + TCD	LOO	0.933 ± 0.000	0.853 ± 0.005	0.342 ± 0.008
	BS	0.920 ± 0.014	0.846 ± 0.011	0.316 ± 0.018
MOCAIP	LOO	0.933 ± 0.000	0.851 ± 0.003	0.339 ± 0.005
	BS	0.925 ± 0.007	0.848 ± 0.008	0.320 ± 0.020
BA	LOO	0.867 ± 0.000	0.516 ± 0.000	0.127 ± 0.000
	BS	0.818 ± 0.009	0.501 ± 0.002	0115 ± 0.001

Se: sensitivity; Spe: specificity; PPV: positive predictivity value; LOO: leave-one out; BS: bootstrapping.

Table 1. Illustration of the CBF classification results.

Besides the metrics that reflect P_3 elevation were selected as classifier features, the metrics including L_t, L_1, L_2, and L_x were also frequently selected. The engagement of L_t in the classification process can be probably explained by the fact that it measures the timing difference between ECG QRS peak and the onset of ICP pulse, which is significantly influenced by systemic arterial blood pressure. Therefore, L_t is a relevant measure as it contains information about the driving pressure of the cerebral blood flow.

3.4 Discussion

We tested the hypothesis that low global CBF may be detected using morphological metrics extracted from the ICP waveforms through a trained classifier. The main finding was that the incorporation of morphological metrics of ICP was able to significantly improve the performance as compared to only using conventional TCD and blood analysis measurements. Although the study was retrospective and data-driven, we believe that it should motivate further studies to investigate the implications and the underlying mechanisms of the association between ICP pulse morphology and cerebral blood perfusion.

One of the findings from the classification experiment is that the elevation of the third peak of an ICP pulse may indicate low global cerebral perfusion. Some questions can be raised regarding whether controlling ICP can also lead to the control of cerebral venous pressure. This is important because the true perfusion pressure is actually determined by the difference between arterial and venous pressure. Even when the mean ICP is well within the prescribed limit, the true perfusion pressure may be still low in situation of cerebral venous hypertension.

4. Predicting intracranial hypertension

Intracranial hypertension (IH) poses a constant threat to head injured patients because it may lead to secondary injuries due to decreased cerebral perfusion pressure and cerebral ischemia. Because bedside monitors are usually designed to report only a short-term history of the ICP, large scale patterns and trends on average ICP that might help to prevent IH are not available to the bedside clinician. Therefore, the constant attention of the nursing staff and their prompt reaction following detecting of an IH episode are critical aspects during the management of patients with IH issues. There is a clear need for a computerized monitoring support that would be accurate in predicting ICP hypertension several minutes ahead, offering enough time to attract the full attention of the bedside clinician.

The main hypothesis is that precursor features can be detected in the ICP signal prior to the elevation. Several studies have verified this hypothesis and offer various insights into which form the predictive features might take. Amplitude of ICP [31, 32], variance of changes [33-35], and rounding of pulse waveform [36] have been shown to correlate with changes of the mean ICP. Decreases in ABP were observed at the beginning of plateau waves [37], and A waves [38]. Moreover, system analysis [39] suggested that a change in the transfer function that relates ABP to ICP may precede elevations. Several other investigators have also attempted to make predictions using wavelet decomposition of the ICP signal [40-42]. More recently, two studies [12, 43] demonstrated that morphological features extracted from the ICP waveform at various times before the elevation onset contains predictive information for IH. Despite more than 30 years [44, 45] of investigation, the automatic, real-time prediction of ICP hypertension is still beyond current methods. Drawing from the studies [12, 36, 43] indicating that ICP morphology contains relevant predictors of IH, we present in this section a framework [65] to predict IH based on morphological features of ICP. A key contribution of this study is to test the effectiveness of ensemble classifiers (AdaBoost, Extremely Randomized Decision Trees) to make temporal prediction. The proposed framework is evaluated on a representative database of 30 neurosurgical patients admitted for various intracranial pressure related conditions.

4.1 Methods

4.1.1 Data source and pre-processing

The dataset of ICP signals originates from the University of California, Los Angeles (UCLA) Medical Center. The ICP and ECG signals were acquired continuously at a rate of 240 Hz or 400 Hz using intraparenchymal sensors from a total of 30 patients treated for various intracranial pressure related conditions. These patients were monitored because of headache

symptoms (idiopathic intracranial hypertension, Chiari syndrome, and slit ventricle patients with clamped shunts) with known risks of ICP elevation.

Intracranial hypertension episodes, defined as an elevated ICP greater than 20 mmHg for a period longer than five minutes, were manually delineated by retrospective analysis. The elevation onset was marked at the beginning of the plateau. From this analysis, 13 patients were identified with at least one IH episode, leading to a total of 70 episodes. Based on the expert review of the ICP signal and the manual annotation of the elevation onset, ICP and ECG segments were extracted to cover the period from 20 minutes before to one minute after the onset.

Control segments were constructed by randomly extracting ten-minute ICP segments from the 17 control patients who did not present a single episode of ICP elevation, and from the IH patients no less than an hour before or after an ICP elevation episode. There were a total of 70 control segments which are evenly distributed among all patients. The 140 IH and NON-IH ICP segments were then processed by MOCAIP so that morphological waveform features were extracted to describe each one minute segments of ICP.

4.2 Experimental setup

The prediction of ICP elevation is posed as a classification problem where each input example $x_i \in X$ is a set of N_s MOCAIP vectors $x_i = \{\alpha_0, \ldots, \alpha_{N_s-1}\}$ calculated over a series of successive one-minute ICP segments. The corresponding output $y_i \in Y$ is a binary variable which equals 1 if the ICP segment led to a treated IH episode. The performance in terms of Area Under the Curve (AUC) is reported for input segments x_i extracted at various time-to-onset for the predictive model. The impact of the number N_s of successive ICP segments used to construct the input vectors $x_i = \{\alpha_0, \ldots, \alpha_{N_s-1}\}$ is evaluated for different prediction techniques. The main purpose of the experiment is to test the hypothesis that the use of ensemble classifiers improves the prediction of IH because it can exploit more efficiently the morphological information contained in longer ICP segments located prior to the elevation onset.

4.2.1 Performance Evaluation by Time-To-Onset Variation

For evaluation, a ten-fold cross-validation at the patient level is performed and three different prediction techniques are compared; Multiple Linear Regression (MLR) [46], Adaptive Boosting (AdaBoost) [47], and Extremely Randomized Decision Trees (Extra Trees) [48]. The models are trained on each fold such that each positive example $x_i = \{\alpha_0, \ldots, \alpha_{N_s-1}\}$ corresponds to the $N_s - 1$ vectors of morphological metrics $\alpha_i \in R^{N_f}$, where Nf = 24 is the number of MOCAIP metrics used in this study. The negative examples are randomly sampled from the pulses of the control set such that the training dataset is balanced and contains an equal number of positive and negative examples. For testing, the models are evaluated on the excluded fold by varying the time-to-onset ρ at which the ICP segments $x_i = \{\alpha_{0+\rho}, \ldots, \alpha_{N_s-1+\rho}\}$ are extracted.

4.2.2 Number of morphological ICP segments

This experiment aims at evaluating if the use of additional morphological vectors extracted up to ten minutes ($N_s = 10$) prior to the tested time-to-onset can improve the prediction performance of the models. To do so, the classifiers are trained such that the input x_i of the positive examples are the N_s morphological vectors $\{\alpha_0, \alpha_1, \ldots, \alpha_{N_s-1}\}$ extracted from the segments prior to the onset plus the segment concurrent to the IH onset. Training of the models is performed for ten different lengths $N_s = \{1, \ldots, 10\}$, from one to ten minutes. Controls of corresponding lengths are randomly extracted from the current fold but remain the same across the different time-to-onset. Each model is evaluated using the average AUC results computed from a ten-fold cross-validation, and ten different time-to-onset $\rho = \{0, \ldots, 9\}$.

4.3 Results

The best results of each method are reported in Fig. 5 in terms of AUC. While the linear classifiers obtain an AUC of $[0.87, 0.78, 0.71]$ for the time-to-onset corresponding to $[1, 3, 6]$ minutes prior to the elevation respectively, the use of ensemble classifiers significantly improves the AUC. AdaBoost reaches an AUC $[0.93, 0.84, 0.80]$, and Extra-Trees performs even better with an AUC of $[0.96, 0.91, 0.87]$.

The Extra-Trees method shows significant improvement in terms of average AUC when the length of the input is increased. For $[1, 5, 10]$ minute(s)-long segments, the AUC is respectively $[0.77, 0.88, 0.9]$. AdaBoost also shows significant increases in AUC, from $[0.75, 0.83, 0.84]$ for segments of $[1, 5, 10]$ minute(s) length, respectively. The linear models are unable to efficiency exploit the larger segments of morphological ICP data. AUC results are $[0.76, 0.65, 0.73]$ for segments of $[1, 5, 10]$ minute(s) length, respectively. The best average AUC for the linear model was observed using a single ICP segment $N_s = 1$. In contrast, the best performance for AdaBoost and Extra-Trees models is obtained with $N_s = 10$ ICP segments, corresponding to ten minutes of ICP data extracted prior to the tested time-to-onset.

Although the previous experiments demonstrate that the ensemble classifier models trained over ten minutes of ICP data perform better than the one trained over shorter segments, it is not clear if each additional one minute ICP segment contribute independently to the improvements, or if they are complementary; in which case the dynamic of change of ICP morphology over time would appear to be useful. To test these hypothesis, three different learning strategy of the Extra-Trees models are compared. The first model (a), which is used as baseline, is trained on a single ($N_s = 1$) one-minute long segment $x_i = \{\alpha_1\}$. The second strategy (b) consists in learning independently ten different models on each one-minute long segment and then fuse their output using an arithemic mean. Finally, (c) is to build a single model trained on a series of ten ($N_s = 10$) one-minute long segments concatenated to a single input vector $x_i = \{\alpha_1, \ldots, \alpha_{10}\}$. Although, the use of ten independent classifiers (b) improves the overall performance versus the use of only one classifier (a), there is an additional increase in AUC by using all ten vectors at the same time (c). This results

indicates that the relative values of successive morphological vectors contain relevant precursors of IH. It is an important finding because it means that the dynamic of ICP changes holds critical predictive information.

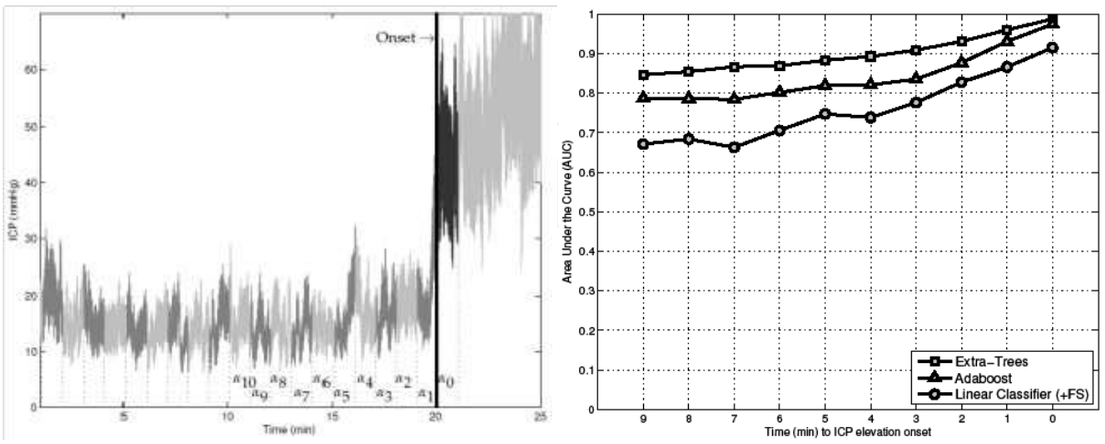

Fig. 5. Illustration of an IH ICP episode (left). Elevated episodes are divided into 21 segments of one minute. For each segment, MOCAIP is applied to extract morphological vectors. On the right, the AUC is reported after a leave-one-out crossvalidation for each technique. Extra-trees ranks first and is followed by the AdaBoost and Multi-linear classifiers (reproduced with permission from [65]).

4.4 Discussion

Thanks to the use of a series of successive one minute ICP segments as input to classifier ensemble techniques, the proposed study has demonstrated that ensemble classifiers can exploit more efficiently the morphological information contained in the pulse. The performance improvement observed in our experiments can be attributed to the following reasons:

- First, as it has been shown in other applications, the two ensemble classifiers perform better than the multiple linear classifier because they can better capture the nonlinearity between the morphological vectors and the outcome.
- Second, the use of a larger segment of ICP segment prior to the onset improves the accuracy.
- Finally, the use of a full sequence of successive morphological vectors at once leads to better models than the one based on individual vectors which indicates that the relative values and the order between successive morphological vectors contain additional precursors.

Although the ICP of brain injured patients is continuously managed by the bedside clinicians, changes in ICP prior to elevation are reflected by complex variations in the morphology of the signal that are difficult to be recognized in real-time. Decision support tools that would alert the bedside clinicians of future ICP elevation would add a new proactive dimension to the current treatment of ICP elevations, which largely remains a reactive procedure. Further improvement of the technical methodology and a better

understanding of the physiological meaning of these morphological variations should be possible. Ideally, we would like to translate the rules learned by ensemble classifiers into a physiological model in an attempt to represent ICP dynamics explicitly.

5. Acute hypercapnic cerebral vasodilatation

The influence of changes within the cerebral vasculature and there impact on ICP remain poorly understood in humans. Studies [49] have shown that in head injured patients, the cerebral perfusion pressure is inversely proportional to the amplitude of pulsatile inflow and, consequently, the exponential shape of the pressure-volume relationship is not the only factor influencing the magnitude of ICP pulse wave [50]. This section presents a recent study [14] conducted by our group to test the hypothesis that acute hypercapnic cerebral vasodilatation induces consistent changes in ICP waveform morphology. This hypothesis is tested on a dataset of ICP signals of uninjured patients undergoing a CO_2 inhalation challenge in which hypercapnia induced acute cerebral vasodilatation. For each morphological metrics extracted from the ICP waveforms using MOCAIP, the consistency and rate of change were analyzed.

5.1 Materials and methods

The hypercapnic dataset consists of the ICP and ECG recordings of four patients, who were admitted at UCLA medical center for the evaluation of their chronic headaches. During their hospitalization, the patients received continuous ICP monitoring using intraparenchymal microsensors situated in the right frontal lobe. They also underwent a CO_2 challenge test by inhaling a 5% CO_2 mixture for less than three minutes. During the test, ICP and ECG signals were recorded at a sampling rate of 400 Hz at the bedside with a dedicated acquisition system.

To quantify the rate of change of each metric over a specific time segment, a line was first fitted to the segment of interest and then the slope of this line was used to calculate the rate of the metric change. The sign of the obtained hourly rate of change (negative vs. positive) was used to determine the trend of change (decreasing vs. increasing).

5.2 Experimental protocol

The average duration of the selected data segment was (5.1 ± 0.7 minutes) which included (1.5 ± 0.5 minutes) of baseline, (2.5 ± 0.5 minutes) of CO_2 challenge test and (1.1 ± 0.2 minutes) of post-test data. The slope of the lines fitted to each of the extracted metrics over the rising edge of ICP signal during CO_2 challenge test and the falling edge of ICP signal during the post-test normal breathing, were used to define the hourly rate of change during the test and post-test normal breathing, respectively. For the purpose of comparing the hourly rate of change between different metrics, each metric rate was normalized by the average value of the corresponding metric over either the last ten beats of the baseline or the first ten beats of the stabilized part of the post-test data.

To evaluate the results from baseline, test, and post-test, we report 1) the consistency of changes of individual metrics; 2) differences in rate of metric changes; and 3) which of the

peak regions (P1, P2 and P3) has a more dramatic change during the cerebral vasodilation; the specifics of how the region assignments were defined are in the publication [14]. In addition, we calculated the region-weighted relative hourly rate of change averaged over the subset of consistent metrics.

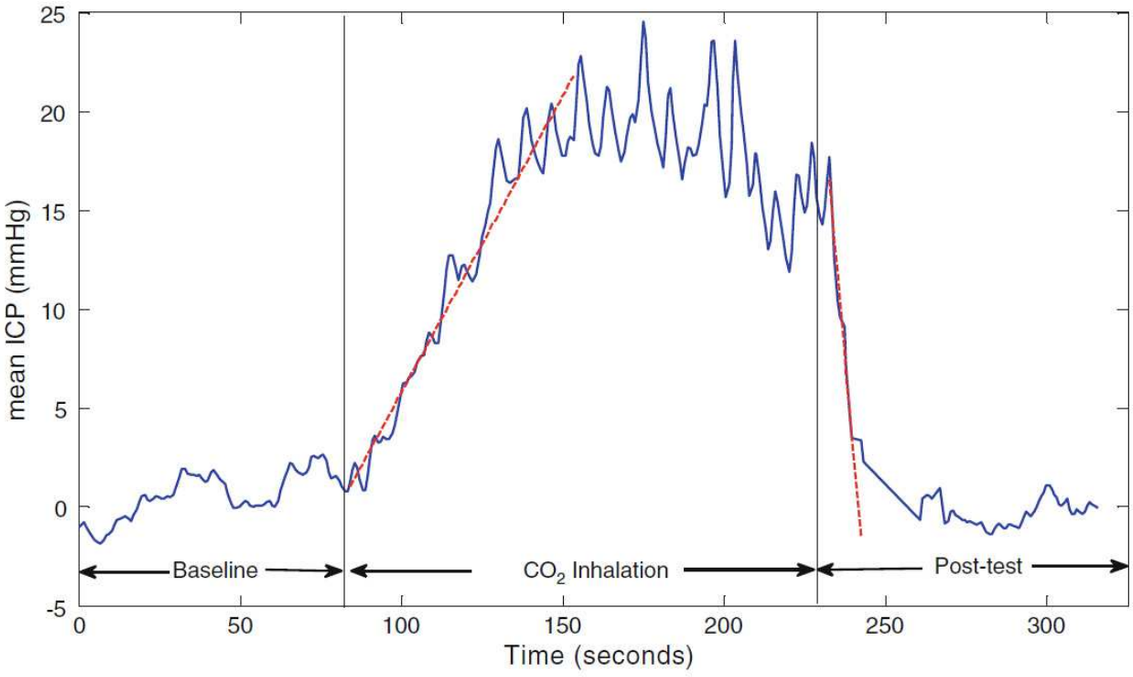

Fig. 6. Illustration of induced hypercapnia for a headache patient. There are three segments (Baseline, CO_2 Inhalation, and Post-test) with the linear fits shown by dotted lines (reproduced with permission from [14]).

5.3 Results

Fig. 6 depicts the mean ICP value for one of the headache patients during the baseline, the CO_2 challenge test, and the post-test normal breathing. When the patient inhales the 5% mixture of CO_2, mean ICP increases over time, reaches a saturation level, and then stabilizes. When the patient returns to breathing normal concentrations of CO_2, the mean ICP returned to baseline in less than one minute.

Investigating the hourly rate of change for all 128 ICP metrics during the hypercapnic and normal breathing post-test data, reveal that; out of 128 ICP metrics, 72 metrics had consistent changes in association with CO_2 changes for all four subjects. We observe that no metrics had the same trend during both the hypercapnic and normal breathing post-test data. This observation is consistent with our expectation that, if a variable has a specific trend of change in one condition, the change would be in the opposite direction as the condition is reversed. We also observe that for all subjects, 50 metrics consistently increased ("+" metrics) during hypercapnia and decreased when patients switched back to room air and 22 metrics consistently decreased ("-" metrics) during CO_2 inhalation phase and increased during post-test normal breathing.

The region-weighted (P1, P2, P3) relative hourly rate of change of the 50 "+" metrics were (0.518, 1.076, and 0.976), respectively. Conversely, for the 22 "-" metrics, the region-weighted relative hourly rate of change averaged over 22 "-" metrics were (0.20, 0.32 and 0.27), respectively.

5.4 Discussion

Acute vasodilatation caused consistent changes in a total of 72 ICP pulse morphological metrics. In addition, it appears that the P_2 sub-region responded to cerebral vascular changes in the most consistent way with the greatest changes as compared to P_1 and P_3 sub-regions. Information with regard to how ICP pulse morphology responds to vasodilatation and vasoconstriction may allow surrogate, continuous monitoring of the cerebral vasculature.

In summary, the present work provides positive preliminary results related to the hypothesis that the dilation/constriction of the cerebral vasculature results in detectable consistent changes in ICP morphological metrics. Acute vasodilatation caused consistent changes in a total of 72 ICP pulse morphological metrics. In addition, it appears that the P_2 sub-region responded to cerebral vascular changes in the most consistent way with the greatest changes as compared to P_1 and P_3 sub-regions.

6. Morphological ICP waveform characteristics during slow waves

The diagnosis and management of NPH remain challenging mostly due to a lack of reliable methods of selecting candidates for shunt implantation and third ventriculostomy. There exists positive [51, 52] and negative [53-55] evidence that frequent presence of ICP slow waves predicts a positive outcome after shunt implant. ICP slow waves, also known as Lundberg's B-waves, are defined as oscillations with a frequency of 2-0.5/minute and large amplitude [56]. There exists indirect evidence that certain characteristics of ICP slow waves may contain useful information for correctly diagnosing NPH and predicting shunt response. It was recently found that increased ICP pulse pressure amplitude has a predictive value for shunt response [9, 57]. In this section, we describe our recent attempt [13] to detect and separate periods of ICP slow waves (BW, “B-wave”) from those of flat or nearly flat ICP (NW, “no wave”) in an overnight ICP recording. We hypothesized that mean values and variations of ICP pulse morphological metrics extracted by the MOCAIP algorithm can be effectively used as input feature vectors to a classification algorithm to distinguish between periods of flat ICP (NW) and those with slow waves (BW). Such a classifier can then be used to construct an automated ICP slow wave recognition algorithm.

6.1 Materials and methods

Pre operative (shunt) overnight ICP recordings performed in 44 patients hospitalized at the UCLA Adult Hydrocephalus Center. Hydrocephalus was diagnosed for all patients. An intraparenchymal ICP sensor was inserted in the right frontal lobe and simultaneous recordings of ICP and ECG signals were performed at a sampling rate of either 400 Hz or 240 Hz. The signal recordings were visually screened by three independent experts to select both BW and NW patterns. Fig. 7 presents an example of ICP overnight monitoring where

initially fairly stable ICP recording transforms into clearly distinguishable slow waves with relatively high amplitude and asymmetrical shape. In our study, small ICP slow waves with amplitude less than six mmHg were classified as NW pattern. As both patterns of ICP (BW and NW) might occur multiple times during overnight monitoring in the same patient, we included several selections from the same study. The total number of selected patterns was 276 (NW-131 and BW- 145).

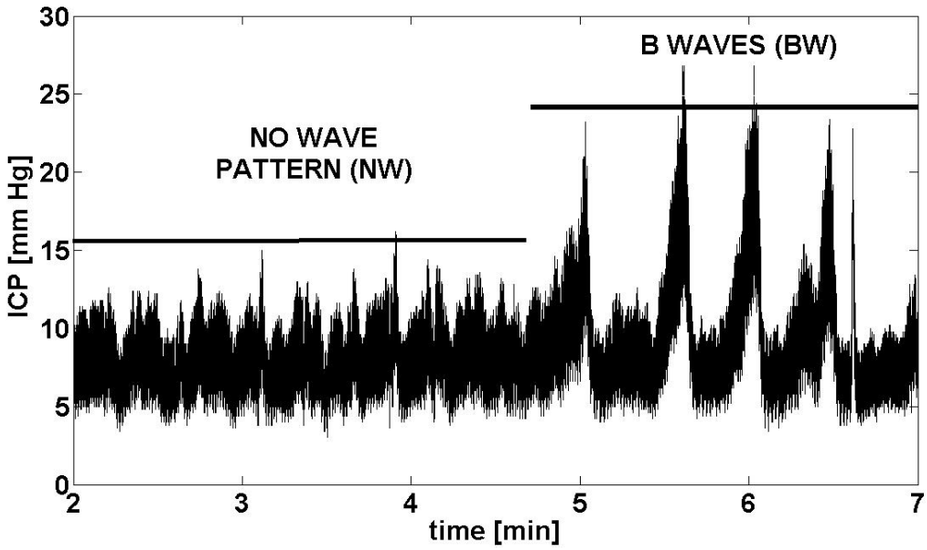

Fig. 7. Illustration of B wave segment (reproduced with permission from [13]).

6.1.1 Feature selection and classification

A total of 48 metrics (comprising 24 morphological metrics plus their standard deviation) were used to described the morphology of each ICP pulse.

To optimize the classification performance, three feature selection techniques (differential evolution (DE), discriminant analysis (DA) and analysis of variance based on Anova (V)) were applied to find an optimal set of MOCAIP metrics under different criteria. In addition, we selected three sets of metrics common to those found by combination of two selection methods, to be used as classification features (differential evolution and analysis of variance, discriminant analysis and analysis of variance, and combination of differential evolution and discriminant analysis).

A regularized linear quadratic classifier was used discriminate between BW from NW based on morphological ICP features. We repeated classification experiment seven times: first time for the set of optimal ICP metrics chosen by DE algorithm, second time for the set of ICP metrics selected based on analysis of variance (V), the third time for these metrics picked by step-wise DA approach, the next three runs were repeated for the metrics overlapped two sets: DE+V, DA+V and DE+DA, and finally we used only one parameter -- S.D. of mean ICP to confirm possible advantage of using combination of metrics over single metric (SM). To compare the performance of classification for different sets of metrics, we ran the bootstrapping procedure 25 times to calculate average and S.D. of performance metrics including Se, Spe, PPV and Ac.

6.1.2 Results and discussion

Results indicate that the changes in six morphological metrics (S.D. of: dP_2, dP_{12}, dP_{13}, $Curv_T$, dICP, mICP) were sufficient to distinguish between BW from NW with high specificity 96.2% and acceptable accuracy 88.9%.

Based on our experiments, using DE in conjunction with Anova to derive the final set of metrics leads to the best classification results. The combination of methods: DA+V as well as DE+DA did not improve the classification performance. Combining DE and V methods appeared to be complementary in our study. Since accuracy of classification experiment for Anova+DE is the highest (88.9%) and the number of input metrics is reasonable small (six metrics), we ranked this method as the best for separating BW from NW.

The final list of six metrics selected by DE+V (S.D. of: dP_2, dP_{12}, dP_{13}, $Curv_T$, dICP, mICP) reflects the most salient changes associated with ICP increase due to slow waves. We found that amplitude of P_2 component notably increases during ICP slow wave occurrence (hence S.D. of dP_2), which is also associated with increase in total curvature of the pulse (hence S.D. of $Curv_T$). Amplitude of P_1, most likely related to systole of arterial pressure [58], shows a moderate increase during BW in comparison with both dP_2 and dP_3 (hence S.D. of dP_{12}, S.D. of dP_{13}).

7. Predicting lumbar drain outcome from ICP morphology

Due to the complication rate and malfuction assoicated with existing shunt technologies, differentiating patient with NPH that will benefit from shunt implantation is significant. Extended lumbar drain (LD) for 72 hours has become a popular pre-shunt workup in many neurosurgical centers [59-61]. Its popularity stems from the findings of an excellent study which demonstrated the high specificity and sensitivity of predicting shunt response based on LD test outcome [60, 62]. However, the mechanistic relationship between positive LD outcome and shunt response remains to be elucidated. Therefore, many centers also employ additional tests to assess patients for predicting their shunt response. Overnight ICP monitoring is one of such tests. It has been reported in many studies that overnight ICP monitoring is able to reveal many phenomena that a short-term ICP monitoring or lumbar puncture cannot reveal, e.g., large but slow oscillations of ICP that are termed B-waves. However, the capability of overnight ICP monitoring to predict shunt response remains controversial. [51, 53-55].

Given these existing contradicting results, elucidating the potential prognostic value of overnight ICP monitoring is significant. Overnight ICP monitoring could be an important economic alternative to LD because it requires a shorter hospital stay for patients if its prognostic value can be fully explored. Unfortunately, many existing analysis methods applied to overnight ICP recordings are very subjective and usually extract limited amounts of information from overnight ICP recordings. On the other hand, a few studies utilizing more advanced ICP signal analysis methods [7, 10] have demonstrated that the amplitude of ICP pulse has excellent predictive value for shunt response. In addition to lack of complex analysis methods of overnight ICP, a potential limit to the existing studies that use shunt response as an end-point is that such outcome

is also determined by many other post-implantation factors not necessarily associated with overnight ICP characteristics.

Therefore, this work aims to develop an automated method of feature extraction and decision rule construction from overnight ICP recording. This method is used to assess the predictive accuracy of LD outcome instead of shunt outcome.

Specifically, we used the MOCAIP algorithm to analyze the overnight ICP recordings. MOCAIP was applied to consecutive short segments of an ICP recording resulting in 128 metrics per each segment. Then various feature functions were designed to summarize the distribution of the 128 metrics from all the segments per each ICP recording. The predictive value of each feature-metric pair was then assessed using the area under curve [60] of the receiver operator characteristic (ROC) curve. Based on the ROC curve, a simple decision rule involving one metric can be derived for predicting LD outcome. To further improve the performance, we proposed an automated way to combine two such rules.

7.1 Materials and methods

The present retrospective study involved 54 patients undergoing pre-shunt workup that included overnight ICP monitoring and extended lumbar drain (three-day) while hospitalized at the UCLA Adult Hydrocephalus Center. An intraparenchymal ICP microsensor (Codman and Schurtleff, Raynaud, MA) was inserted in the right frontal lobe and monitoring started at least one night before the placement of the LD. Continuous waveform data including ECG and ICP was captured using the BedMaster system with a sampling rate of 240 Hz. Patients were assessed both pre-LD and post-LD before discharge from the hospital by ten meter walking exam, and an NPH routine assessment which includes the Mini-mental state examination (MMSE). The LD outcome used in the present work was retrospectively collected as indicated from the clinical report of the follow-up visit after the LD procedure and predominantly focused on the improvement in gait. The average age and standard deviation of the 54 patients is 72.05 ± 9.63 years respectively, with a gender distribution of 35 males and 19 females. Among the patient cohort, 12 patients (seven males and five females) showed no improvement in gait following the procedure.

7.2 Feature functions

Once the metrics for each dominant pulse have been computed an additional processing step is used to summarize each of the 128 MOCAIP metrics for one overnight ICP recording via five feature functions. For example, if a patient has ten hours of continuous ICP data there will be approximately 1200 dominant pulses, for each dominant pulse there is 128 MOCAIP metrics, each of the MOCAIP metrics can be summarized with the five feature functions (below). There is no prior knowledge with regard to the best way of summarizing an overnight ICP recording. Therefore, it is necessary to allow for an automated process to identify the best candidates. We have evaluated the following feature functions:

Average feature: This feature function simply calculates the average of each individual metric across one overnight ICP recording.

Standard deviation feature: This function calculates the standard deviation of each individual metric across one overnight ICP recording.

Percentage feature: This function calculates the percentage of time when a metric is greater than a threshold. This threshold is determined by pooling data from all patients and then determined as the average of the corresponding MOCAIP metric.

Percentage of standard deviation feature: This function calculates the percentage of time of the standard deviation of MOCAIP metrics greater than a threshold calculated from a five-minute ICP. The threshold was determined as the standard deviation of pooled MOCAIP metrics from all patients.

Range feature: This function calculates the difference between the 95 percentile and the 5 percentile of each individual metric of an overnight ICP recording.

7.3 Optimal single-metric rule

After applying a feature function, an overnight ICP recording is reduced to a vector of 128 metric-feature pairs. We next seek for a single-metric rule to predict LD outcome in the following form: if a metric-feature of an overnight recording is greater (or smaller) than a threshold, then LD outcome will be positive. Note, rules published in several existing studies [10, 63] can be considered as specific instances of the above form. For each metric-feature, we generate a sequence of threshold values by pooling all the data. This sequence of threshold values can be used to generate two ROC curves for each metric-feature, one of which corresponds to the greater than situation and another of which corresponds to the less than situation. Then we retain the ROC that has an AUC greater than 0.5 and discard the other for each metric. Next, for each feature the optimal metric is defined as the one with the greatest AUC. The impact of the optimal metric selection (as a function of AUC) is explained in the results section. Following the optimal metric determination for each feature, one natural step further is to determine if one can combine two such rules to obtain a better performance (a combination of two of the five features described above). Considering the combination of two features (A and B) with the corresponding set of false positive, true positive, false negative, and true negative cases represented (from rule A) as FPA, TPA, FNA, TNA, respectively, the notation is analogous for rule B. Furthermore, we shall consider two possible combination operations: AND and OR. If the OR operator is used for combination, then the resultant sets of false positive, true positive, false negative, and true negative are FPA ∪ FPB, TPA ∪ TPB, FNA ∩ FNB, and TNA ∩ TNB. On the other hand, if the AND operator is used for combination, then the corresponding sets are FPA ∩ FPB, TPA ∩ TPB, FNA ∪ FNB, and TNA ∪ TNB. Based on this analysis, the accuracy of the combined predictive rules can be calculated using their respective true positive and true negative values along with the total number of patients. Therefore, one can choose the combinations with the maximal accuracy.

7.4 Data analysis protocol

In this section, we summarize the data analysis protocol used in the present work to determine the best rule combination and its accuracy. The following steps were taken to analyze the 54 overnight ICP recordings:

1. Each recording is analyzed using the MOCAIP algorithm on consecutive 30-second segments.
2. Resultant MOCAIP metrics are then manually checked for any errors in recognizing legitimate dominant pulse and placement of the landmarks. This step is facilitated by using software developed in house.
3. Generate the threshold sequence for each metric that will be used to generate ROC curve. The i-th value of the sequence of thresholds is calculated for each metric-feature by the following equations: (i-1) where L is the mean plus the ten standard deviation of the metric-feature divided by the number of steps, which is 100 in the present work.
4. Each value of the threshold sequence is used to form two simple rules (greater than and less than), which are then used to assess the 54 cases. The corresponding false positive rate (FPR) and true positive rate (TPR) are obtained. After sweeping through the sequence, two ROC curves are obtained but only the one with AUC greater 0.5 is retained.
5. Determine the optimal metric-feature. This is achieved by selecting one metric-feature that has the largest AUC per each feature function evaluated. In other words, for each feature defined above, the metric (out of the 128 calculated by MOCAIP) with the greatest AUC is defined as the optimal metric-feature (five total, one for each feature).
6. Determine the rule. For the optimal metric-feature, the optimal point on the ROC curve is selected as the operating point, which gives a false positive rate less than 0.35.
7. Then the accuracy of the ten pairs (two combination rules and five feature) are calculated.
8. The best rule combination is then determined as the one with the greatest accuracy.

7.5 Results

Panel F of Fig. 8 displays ROC curves of each of the 128 metric-features (average feature function is used here as an example). The ROC curve shown in bold represents the metric with the greatest AUC; which was selected as the optimal metric-feature for rule construction. The ROC curves of optimal metric-pair corresponding to each of the five feature functions (A: Average feature function; B: Standard deviation feature function; C: Percentage of average feature function; D: Percentage of five-minute standard deviation feature function; E: Inter 5-95 percentile feature function) are shown in Panels A through E of Fig. 8 where the selected MOCAIP metric is also spelled out. On each curve, the operating point is circled, which corresponds to the particular threshold value selected for rule construction.

In summary, the individual metric-feature rules found in the present work are: 1.If standard deviation of RLv2p2Lp1p2 of overnight ICP recording is > 0.0547, then patient will respond to LD. 2.If average RCurvp3Curvv2 of overnight ICP recording is > 0.9808, then patient will respond to LD. 3.If percentage of RC1 of overnight ICP recording greater than 8.76 is < 41.48%, then patient will respond to LD. 4.If percentage of five minute segments of ICP having a standard deviation of RRC3k2 greater than 57.68 is > 0.49%, then patient will respond to LD drain. 5.If the inter 95-5 quartile range of RCurvp2Curvp3 of overnight ICP recording is < 64.25, then patient will respond to LD. The accuracy for the corresponding features is: 70.4%, 72.2%, 74.1%, 72.2%, and 79.6% respectively. Finally, the OR combination of rules 4 and 5 achieves the best accuracy of 88.9%.

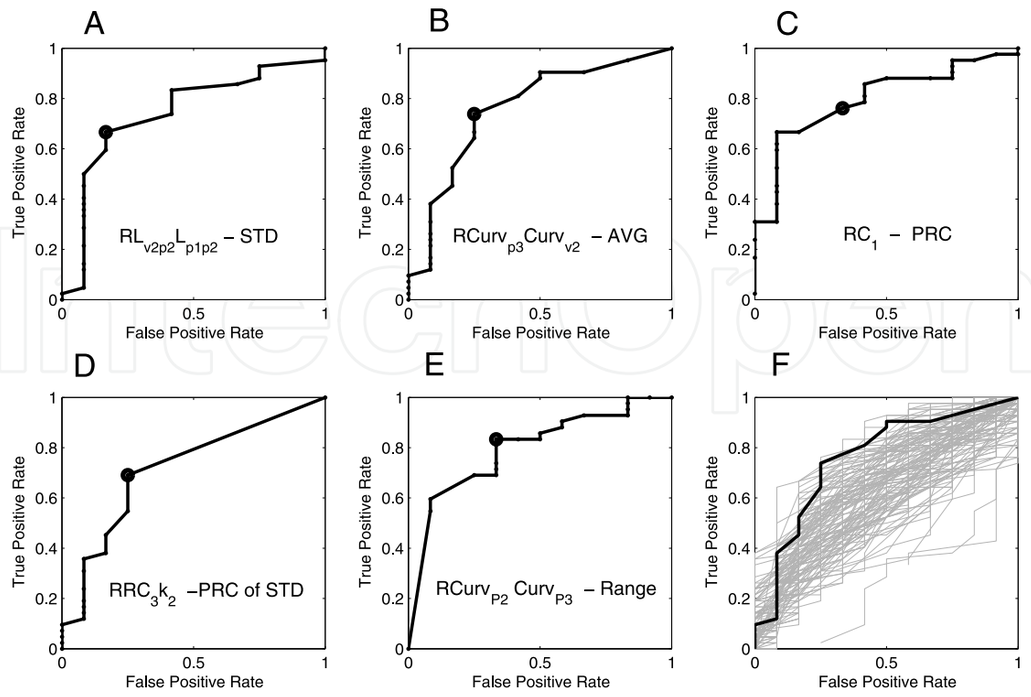

Fig. 8. Illustration of LD ROCs (reproduced with permission from [67]).

7.6 Discussion

We have demonstrated a systemic way of deriving two-rule combination of simple decision rules from overnight ICP recording to predict the corresponding outcome of three-day LD for patients with NPH clinical triad undergoing pre-shunt evaluation. Using a cohort of 54 patients, we are able to find optimal two-rule combination that reaches an accuracy of 88.9%. This rule can be explained in plain English such that it can be readily communicated to non-technical clinicians and patients. Although further validation with large patient cohort is needed, technically, the rules found in the present work in combination with an automated analysis of overnight ICP using the existing MOCAIP algorithm can readily be built into a decision support system of NPH diagnosis and evaluation that has the potential to reduce the time and cost associated with the existing three-day LD procedure.

A systemic way of discovering predictive rules is needed if a large number of ICP pulse morphological metrics are involved to construct rules. Compared to the existing studies that focus on either mICP or ICP pulse amplitude, the increased number of ICP metrics demands an objective way of discovering rules to guarantee optimality and avoid bias. Indeed, the five individual optimal metrics found in the present work do not include either mean ICP or ICP wave amplitude demonstrating the potential power of adopting a more comprehensive ICP pulse morphology characterization.

The proposed rule discovery framework can be easily extended in several aspects. We have proposed five simple feature functions to summarize an overnight ICP recording. More complex feature function can certainly be implemented in future work. In particular, we believe that feature functions characterizing the relationship among MOCAIP metrics could potentially offer better predictive power as compared to single-metric feature functions used

here. Furthermore, we have only studied the combination of two rules, one could readily derive the equations to calculate the accuracy of combining multiple rules and check if the predictive accuracy can be further improved.

One fundamental limitation of the present work is the lack of cases to conduct independent evaluation of the discovered rules. It therefore remains to be demonstrated whether the same level of predictive accuracy can be retained when applying the rules discovered using our dataset to process data from other centers and how the data from multi-centers can be utilized to refine the rules. The present work has clearly demonstrated the technical feasibility of such future studies and hopefully more precise and robust predictive rules can be discovered through multi-center collaboration and the adoption of advanced ICP signal analysis and data mining methods.

8. Conclusions

Pulse pressure amplitude has been linked to several conditions with promising results in NPH for predicting shunt responsiveness [9, 10]. Work has also been done in chronic headaches; again, showing the usefulness of pulse pressure amplitude. Recent, detailed pulse pressure morphology analysis by our group has shown promise as a possible indicator of low global cerebral blood perfusion [11]. The resistance from many clinicians and researchers is the unknown relationship between these pulse pressure metrics (MOCAIP) and their physiologic meaning. Therefore, the additional information provided by knowing the origins of these pulse pressure features would help bridge the gap between a strictly data mining approach and physiologic meaning. Finally, the importance of this work was confirmed in a recent review article by Wagshul et al.:

"Given the success of invasive pulsatility measurements in clinical prognosis, studies which can provide a link between changes in pulse pressure and changes in non-invasive TCD- or MRI-based measures of pulsatility will be particularly valuable." [64]

9. Acknowledgements

The work presented in this chapter was supported in part by the National Institute of Neurological Disorders and Stroke (NINDS) and grants R21-NS055998, R21-NS055045, R21-NS059797, R01-NS054881, R01-NS066008, along with a research fund for international young scientists NSFC-31050110122.

10. References

[1] E. A. Bering, Jr., "Choroid plexus and arterial pulsation of cerebrospinal fluid; demonstration of the choroid plexuses as a cerebrospinal fluid pump," *AMA Arch Neurol Psychiatry,* vol. 73, pp. 165-72, Feb 1955.

[2] R. J. Adolph, H. Fukusumi, and N. O. Fowler, "Origin of cerebrospinal fluid pulsations," *Am J Physiol,* vol. 212, pp. 840-6, Apr 1967.

[3] J. Y. Fan, C. Kirkness, P. Vicini, R. Burr, and P. Mitchell, "Intracranial pressure waveform morphology and intracranial adaptive capacity," *Am J Crit Care,* vol. 17, pp. 545-54, Nov 2008.

[4] O. Hirai, H. Handa, M. Ishikawa, and S. H. Kim, "Epidural pulse waveform as an indicator of intracranial pressure dynamics," *Surg Neurol,* vol. 21, pp. 67-74, Jan 1984.

[5] E. R. Cardoso, J. O. Rowan, and S. Galbraith, "Analysis of the cerebrospinal fluid pulse wave in intracranial pressure," *J Neurosurg,* vol. 59, pp. 817-21, Nov 1983.

[6] J. Hamer, E. Alberti, S. Hoyer, and K. Wiedemann, "Influence of systemic and cerebral vascular factors on the cerebrospinal fluid pulse waves," *J Neurosurg,* vol. 46, pp. 36-45, Jan 1977.

[7] P. K. Eide, "A new method for processing of continuous intracranial pressure signals," *Med Eng Phys,* vol. 28, pp. 579-87, Jul 2006.

[8] X. Hu, P. Xu, D. J. Lee, V. Paul, and M. Bergsneider, "Morphological changes of intracranial pressure pulses are correlated with acute dilatation of ventricles," *Acta Neurochir Suppl,* vol. 102, pp. 131-6, 2008.

[9] P. K. Eide and A. Brean, "Intracranial pulse pressure amplitude levels determined during preoperative assessment of subjects with possible idiopathic normal pressure hydrocephalus," *Acta Neurochir (Wien),* vol. 148, pp. 1151-6; discussion 1156, Nov 2006.

[10] P. K. Eide and W. Sorteberg, "Diagnostic intracranial pressure monitoring and surgical management in idiopathic normal pressure hydrocephalus: a 6-year review of 214 patients," *Neurosurgery,* vol. 66, pp. 80-91, Jan 2006.

[11] X. Hu, T. Glenn, F. Scalzo, M. Bergsneider, C. Sarkiss, N. Martin, and P. Vespa, "Intracranial pressure pulse morphological features improved detection of decreased cerebral blood flow," *Physiol Meas,* vol. 31, pp. 679-95, May 2010.

[12] R. Hamilton, P. Xu, S. Asgari, M. Kasprowicz, P. Vespa, M. Bergsneider, and X. Hu, "Forecasting intracranial pressure elevation using pulse waveform morphology," *Conf Proc IEEE Eng Med Biol Soc,* vol. 2009, pp. 4331-4, 2009.

[13] M. Kasprowicz, S. Asgari, M. Bergsneider, M. Czosnyka, R. Hamilton, and X. Hu, "Pattern recognition of overnight intracranial pressure slow waves using morphological features of intracranial pressure pulse," *J Neurosci Methods,* vol. 190, pp. 310-8, Jul 15 2010.

[14] S. Asgari, M. Bergsneider, R. Hamilton, P. Vespa, and X. Hu, "Consistent changes in intracranial pressure waveform morphology induced by acute hypercapnic cerebral vasodilatation," *Neurocrit Care,* vol. 15, pp. 55-62, Aug.

[15] T. Ellis, J. McNames, and M. Aboy, "Pulse morphology visualization and analysis with applications in cardiovascular pressure signals," *IEEE Trans Biomed Eng,* vol. 54, pp. 1552-9, Sep 2007.

[16] H. Takizawa, T. Gabra-Sanders, and J. D. Miller, "Changes in the cerebrospinal fluid pulse wave spectrum associated with raised intracranial pressure," *Neurosurgery,* vol. 20, pp. 355-61, Mar 1987.

[17] M. Aboy, J. McNames, T. Thong, D. Tsunami, M. S. Ellenby, and B. Goldstein, "An automatic beat detection algorithm for pressure signals," *IEEE Trans Biomed Eng,* vol. 52, pp. 1662-70, Oct 2005.

[18] X. Hu, P. Xu, F. Scalzo, P. Vespa, and M. Bergsneider, "Morphological clustering and analysis of continuous intracranial pressure," *IEEE Trans Biomed Eng,* vol. 56, pp. 696-705, Mar 2009.

[19] F. Scalzo, P. Xu, S. Asgari, M. Bergsneider, and X. Hu, "Regression analysis for peak designation in pulsatile pressure signals," *Med Biol Eng Comput,* vol. 47, pp. 967-77, Sep 2009.

[20] F. Scalzo, S. Asgari, S. Kim, M. Bergsneider, and X. Hu, "Robust peak recognition in intracranial pressure signals," *Biomed Eng Online,* vol. 9, p. 61, 2010.

[21] X. Hu, P. Xu, D. J. Lee, P. Vespa, K. Baldwin, and M. Bergsneider, "An algorithm for extracting intracranial pressure latency relative to electrocardiogram R wave," *Physiol Meas,* vol. 29, pp. 459-71, Apr 2008.

[22] V. X. Afonso, W. J. Tompkins, T. Q. Nguyen, and S. Luo, "ECG beat detection using filter banks," *IEEE Trans Biomed Eng,* vol. 46, pp. 192-202, Feb 1999.

[23] Kaufman, Leonard, Rousseeuw, and J. Peter, *Finding groups in data : an introduction to cluster analysis of Wiley series in probability and mathematical statistics*. Hoboken, N.J: Wiley, 2005.

[24] F. Scalzo, S. Asgari, S. Kim, M. Bergsneider, and X. Hu, "Bayesian tracking of intracranial pressure signal morphology," *Artif Intell Med,* Oct 2 2011.

[25] E. Sudderth, A. Ihler, W. T. Freeman, and A. S. Willsky, "Nonparametric Belief Propagation," in *IEEE Computer Society Conference on Computer Vision and Pattern Recognition (CVPR)*, 2003, pp. 605-612

[26] E. Parzen, " On Estimation of a Probability Density Function and Mode," *The Annals of Mathematical Statistics,* vol. 33, pp. 1065-1076, 1962.

[27] W. Obrist and D. Marion, "Xenon techniques for CBF measurement in clinical head injury," *Neurotrauma,* 1995.

[28] R. Aaslid, T. M. Markwalder, and H. Nornes, "Noninvasive transcranial Doppler ultrasound recording of flow velocity in basal cerebral arteries," *J Neurosurg,* vol. 57, pp. 769-74, Dec 1982.

[29] J. Friedman, " Regularized Discriminant-Analysis," *J Am Stat Assoc,* 1989.

[30] R. Storn and K. Price, "Differential evolution - a simple and efficient heuristic for global optimization over continuous spaces," *J Global Optim,* 1997.

[31] J. McNames, C. Crespo, J. Bassale, M. Aboy, M. Ellenby, S. Lai, and B. Goldstein, "Sensitive Precursors to Acute Episodes of Intracranial Hypertension," in *4th International Workshop Biosignal Interpretation*, 2002.

[32] J. Szewczykowski, P. Dytko, A. Kunicki, J. Korsak-Sliwka, S. Sliwka, J. Dziduszko, and B. Augustyniak, "Determination of critical ICP levels in neurosurgical patients: A statistical approach," *Intracranial Pressure II,* pp. 392-393, 1975.

[33] R. Hornero, M. Aboy, D. Abasolo, J. McNames, and B. Goldstein, "Interpretation of approximate entropy: analysis of intracranial pressure approximate entropy during acute intracranial hypertension," *IEEE Trans Biomed Eng,* vol. 52, pp. 1671-80, Oct 2005.

[34] X. Hu, C. Miller, P. Vespa, and M. Bergsneider, "Adaptive computation of approximate entropy and its application in integrative analysis of irregularity of heart rate

variability and intracranial pressure signals," *Med Eng Phys,* vol. 30, pp. 631-9, Jun 2008.

[35] J. Turner, D. McDowall, R. Gibson, and H. Khaili, "Computer analysis of intracranial pressure measurements: Clinical value and nursing response," *Intracranial Pressure III,* pp. 283-287, 1976.

[36] H. D. Portnoy and M. Chopp, "Cerebrospinal fluid pulse wave form analysis during hypercapnia and hypoxia," *Neurosurgery,* vol. 9, pp. 14-27, Jul 1981.

[37] M. Czosnyka, P. Smielewski, S. Piechnik, E. A. Schmidt, P. G. Al-Rawi, P. J. Kirkpatrick, and J. D. Pickard, "Hemodynamic characterization of intracranial pressure plateau waves in head-injury patients," *J Neurosurg,* vol. 91, pp. 11-9, Jul 1999.

[38] M. Rosner, "Pathophysiology and management of increased intracranial pressure," *Neurosurgical Intensive Care,* pp. 57-112, 1993.

[39] I. R. Piper, J. D. Miller, N. M. Dearden, J. R. Leggate, and I. Robertson, "Systems analysis of cerebrovascular pressure transmission: an observational study in head-injured patients," *J Neurosurg,* vol. 73, pp. 871-80, Dec 1990.

[40] M. Swiercz, Z. Mariak, J. Krejza, J. Lewko, and P. Szydlik, "Intracranial pressure processing with artificial neural networks: prediction of ICP trends," *Acta Neurochir (Wien),* vol. 142, pp. 401-6, 2000.

[41] B. Azzerboni, G. Finocchio, M. Ipsale, F. La Forestal, and F. C. Morabito, "Intracranial Pressure Signals FOrecasting with Wavelet Transform and Neuro-Fuzzy Network," in *EMBS-BMES conference* Houston, TX, USA, 2002.

[42] F. Tsui, M. Sun, C. Li, and R. Sclabasi, "A Waveelet Based Neural Network For Prediction of ICP Signal," in *IEEE EMBC*, 1995, pp. 1045-1046.

[43] X. Hu, P. Xu, S. Asgari, P. Vespa, and M. Bergsneider, "Forecasting ICP elevation based on prescient changes of intracranial pressure waveform morphology," *IEEE Trans Biomed Eng,* vol. 57, pp. 1070-8, May 2010.

[44] R. Allen, "Time series methods in the monitoring of intracranial pressure. Part 1: Problems, suggestions for a monitoring scheme and review of appropriate techniques," *J Biomed Eng,* vol. 5, pp. 5-18, Jan 1983.

[45] D. Price, R. Dugdale, and J. Mason, "The control of ICP using three asynchronous closed loop," *Intracranial Pressure IV,* pp. 395-399, 1980.

[46] S. Chatterjee and A. S. and Hadi, "Influential observations, high leverage points and outliers in linear regression," *Statistical Science,* vol. 1, pp. 379-393, 1986.

[47] R. Schapire, "The Strength of Weak Learnability," *Mach. Learn,* vol. 5, pp. 197--227, 1990.

[48] P. Geurts, D. Ernst, and L. Wehenkel, "Extremely randomized trees," *Mach Learn,* vol. 63, pp. 3-42, 2006.

[49] K. H. Chan, J. D. Miller, N. M. Dearden, P. J. Andrews, and S. Midgley, "The effect of changes in cerebral perfusion pressure upon middle cerebral artery blood flow velocity and jugular bulb venous oxygen saturation after severe brain injury," *J Neurosurg,* vol. 77, pp. 55-61, Jul 1992.

[50] M. Czosnyka, E. Guazzo, M. Whitehouse, P. Smielewski, Z. Czosnyka, P. Kirkpatrick, S. Piechnik, and J. D. Pickard, "Significance of intracranial pressure waveform

analysis after head injury," *Acta Neurochir (Wien),* vol. 138, pp. 531-41; discussion 541-2, 1996.

[51] C. Raftopoulos, C. Chaskis, F. Delecluse, F. Cantraine, L. Bidaut, and J. Brotchi, "Morphological quantitative analysis of intracranial pressure waves in normal pressure hydrocephalus," *Neurol Res,* vol. 14, pp. 389-96, Dec 1992.

[52] L. Symon and N. W. Dorsch, "Use of long-term intracranial pressure measurement to assess hydrocephalic patients prior to shunt surgery," *J Neurosurg,* vol. 42, pp. 258-73, Mar 1975.

[53] H. Stephensen, N. Andersson, A. Eklund, J. Malm, M. Tisell, and C. Wikkelso, "Objective B wave analysis in 55 patients with non-communicating and communicating hydrocephalus," *J Neurol Neurosurg Psychiatry,* vol. 76, pp. 965-70, Jul 2005.

[54] M. A. Williams, A. Y. Razumovsky, and D. F. Hanley, "Comparison of Pcsf monitoring and controlled CSF drainage diagnose normal pressure hydrocephalus," *Acta Neurochir Suppl,* vol. 71, pp. 328-30, 1998.

[55] G. F. Woodworth, M. J. McGirt, M. A. Williams, and D. Rigamonti, "Cerebrospinal fluid drainage and dynamics in the diagnosis of normal pressure hydrocephalus," *Neurosurgery,* vol. 64, pp. 919-25; discussion 925-6, May 2009.

[56] N. Lundberg, "Continuous recording and control of ventricular fluid pressure in neurosurgical practice," *Acta Psychiatr Scand Suppl,* vol. 36, pp. 1-193, 1960.

[57] M. Czosnyka, Z. Czosnyka, N. Keong, A. Lavinio, P. Smielewski, S. Momjian, E. A. Schmidt, G. Petrella, B. Owler, and J. D. Pickard, "Pulse pressure waveform in hydrocephalus: what it is and what it isn't," *Neurosurg Focus,* vol. 22, p. E2, 2007.

[58] E. Carrera, D. J. Kim, G. Castellani, C. Zweifel, Z. Czosnyka, M. Kasparowicz, P. Smielewski, J. D. Pickard, and M. Czosnyka, "What shapes pulse amplitude of intracranial pressure?," *J Neurotrauma,* vol. 27, pp. 317-24, Feb 2010.

[59] L. S. Governale, N. Fein, J. Logsdon, and P. M. Black, "Techniques and complications of external lumbar drainage for normal pressure hydrocephalus," *Neurosurgery,* vol. 63, pp. 379-84; discussion 384, Oct 2008.

[60] A. Marmarou, H. F. Young, G. A. Aygok, S. Sawauchi, O. Tsuji, T. Yamamoto, and J. Dunbar, "Diagnosis and management of idiopathic normal-pressure hydrocephalus: a prospective study in 151 patients," *J Neurosurg,* vol. 102, pp. 987-97, Jun 2005.

[61] R. Walchenbach, E. Geiger, R. T. Thomeer, and J. A. Vanneste, "The value of temporary external lumbar CSF drainage in predicting the outcome of shunting on normal pressure hydrocephalus," *J Neurol Neurosurg Psychiatry,* vol. 72, pp. 503-6, Apr 2002.

[62] A. Marmarou, M. Bergsneider, P. Klinge, N. Relkin, and P. M. Black, "The value of supplemental prognostic tests for the preoperative assessment of idiopathic normal-pressure hydrocephalus," *Neurosurgery,* vol. 57, pp. S17-28; discussion ii-v, Sep 2005.

[63] P. K. Eide and A. Brean, "Cerebrospinal fluid pulse pressure amplitude during lumbar infusion in idiopathic normal pressure hydrocephalus can predict response to shunting," *Cerebrospinal Fluid Res,* vol. 7, p. 5, 2010.

[64] M. E. Wagshul, P. K. Eide, and J. R. Madsen, "The pulsating brain: A review of experimental and clinical studies of intracranial pulsatility," *Fluids Barriers CNS,* vol. 8, p. 5, 2011.

[65] F. Scalzo, R. Hamilton, S. Asgari, S. Kim, and X. Hu. Intracranial Hypertension Prediction using Extremely Randomized Decision Trees. *Med Eng Phys*. In press, 2011.

[66] S. Kim, X. Hu, D. McArthur, R. Hamilton, M. Bergsneider, T. Glenn, N. Martin, and P. Vespa, "Inter-Subject Correlation Exists Between Morphological Metrics of Cerebral Blood Flow Velocity and Intracranial Pressure Pulses," *Neurocrit Care*, Dec 7 2010.

[67] X. Hu, R. Hamilton, K. Baldwin, P. Vespa, and M. Bergsneider, "Automated Extraction of Decision Rules for Predicting Lumbar Drain Outcome by Analyzing Overnight Intracranial Pressure," *Acta Neurochir Suppl*, vol. 114, In press, 2011.

IntechOpen

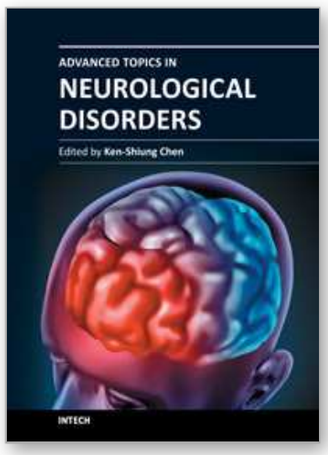

Advanced Topics in Neurological Disorders

Edited by Dr Ken-Shiung Chen

ISBN 978-953-51-0303-5
Hard cover, 242 pages
Publisher InTech
Published online 16, March, 2012
Published in print edition March, 2012

This book presents recent advances in the field of Neurological disorders research. It consists of 9 chapters encompassing a wide range of areas including bioengineering, stem cell transplantation, gene therapy, proteomic analysis, alternative treatment and neuropsychiatry analysis. It highlights the development of multiple discipline approaches in neurological researches. The book brings together leading researchers in neurological disorders and it presents an essential reference for researchers working in the neurological disorders, as well as for students and industrial users who are interested in current developments in neurological researches.

How to reference

In order to correctly reference this scholarly work, feel free to copy and paste the following:

Fabien Scalzo, Robert Hamilton and Xiao Hu (2012). Real-Time Analysis of Intracranial Pressure Waveform Morphology, Advanced Topics in Neurological Disorders, Dr Ken-Shiung Chen (Ed.), ISBN: 978-953-51-0303-5, InTech, Available from: http://www.intechopen.com/books/advanced-topics-in-neurological-disorders/real-time-analysis-of-intracranial-pressure-waveform-morphology

INTECH
open science | open minds

InTech Europe
University Campus STeP Ri
Slavka Krautzeka 83/A
51000 Rijeka, Croatia
Phone: +385 (51) 770 447
Fax: +385 (51) 686 166
www.intechopen.com

InTech China
Unit 405, Office Block, Hotel Equatorial Shanghai
No.65, Yan An Road (West), Shanghai, 200040, China
中国上海市延安西路65号上海国际贵都大饭店办公楼405单元
Phone: +86-21-62489820
Fax: +86-21-62489821

© 2012 The Author(s). Licensee IntechOpen. This is an open access article distributed under the terms of the Creative Commons Attribution 3.0 License, which permits unrestricted use, distribution, and reproduction in any medium, provided the original work is properly cited.

IntechOpen

IntechOpen